Int. J. Electrochem. Sci., 17 **(2022)** Article Number: 220445, doi: 10.20964/2022.04.55

International Journal of
ELECTROCHEMICAL
SCIENCE
www.electrochemsci.org

Short Communication

The Drug Domperidone as a Corrosion Inhibitor for X60 Steel in Hydrochloric Acid Solution

Yanxia Liu[1], *Xiuquan Yao*[2,*], *Chunlin Liu*[3], *Xiaofang Luo*[4], *Chao Guo*[5], *Wei Du*[6]

[1] College of Chemistry and Chemical Engineering, Jining Normal University, Ulanqab 012000, China.
[2] National Center for Materials Service Safety, University of Science and Technology Beijing, Beijing, 100083, China
[3] Latin America Branch, China Petroleum Engineering & Construction Corporation (CPECC), Beijing, 100120, China
[4] China Chongqing Academy of Metrology and Quality Inspection, Chongqing, 402160, China.
[5] Compact Strip Plant, BaoTou Iron and Steel Co., Ltd., Baotou Inner Mongolia, 014010, China.
[6] Metals and Chemistry Research Institute, China Academy of Railway Sciences Corporation Limited, Beijing, 100081, China.
[*]E-mail: b20180439@xs.ustb.edu.cn

Received: 4 January 2022 / *Accepted:* 5 February 2022 / *Published:* 4 March 2022

Electrochemical and SEM methods were used to study domperidone (DPD) as an organic corrosion inhibitor for X60 carbon steel in 1 M hydrochloric acid solution. The corrosion inhibition rate decreases with increasing corrosion inhibitor concentration. The inhibition efficiency was the highest when 400 mg/L DPD inhibitor was added, showing a type of mixed inhibitor. The adsorption of DPD inhibitor on the steel surface conforms to the Langmuir isotherm as a combination of physical and chemical adsorption. In addition, the adsorption conformation of the inhibitor molecules on the steel surface was analyzed by MD calculations and the adsorption energy was calculated.

Keywords: X60; DPD; Hydrochloric acid solution; Electrochemistry; MD calculation

1. INTRODUCTION

Metals, especially steel, play an irreplaceable role in our daily lives and industrial production today due to their excellent mechanical properties, low cost and ease of recycling. Unfortunately, however, steel is sensitive to environmental conditions such as air humidity, oxygen content, acidity and alkalinity and is susceptible to erosion [1, 2]. And these conditions are widely present in the case of pickling, mainly to eliminate local deposits. Corrosion of metals can cause major accidents, seriously threatening the safety of life and property and requiring costly repairs [3, 4]. Among many available protection measures, adding corrosion inhibitor is the most convenient and effective one [5-10].

Inorganic corrosion inhibitors, although excellent protective performance, but its harmful to the environment and human body, gradually replaced by organic corrosion inhibitors. Organic compounds containing heteroatoms such as oxygen, nitrogen and sulfur, whose polar heteroatomic components (usually containing lone pairs of electrons) interact with the cations on the metal surface by adsorption, have a good inhibitory effect on the corrosion of metallic materials, thus slowing down the rate of anodic and cathodic reactions occurring during the electrochemical process [11-15].

In recent years, many drugs have been used as green corrosion inhibitors [15-23]. Domperidone is widely used as a common drug in the pharmaceutical industry. Domperidone contains multiple N atoms in its molecular structure, so it is thought to be a potential corrosion inhibitor with excellent protective effect. In this work, the anti-corrosion ability of Domperidone against X60 steel was verified by adding different concentrations of Domperidone to hydrochloric acid solution. The protective effect of DPD molecules on X60 steel was investigated using electrochemical experiments combined with surface morphology observation, and molecular dynamics calculations were used to theoretically explain the relationship between the molecular structure and the adsorption mechanism.

2. EXPERIMENTAL

2.1 Materials and solutions

Domperidone (DPD) was purchased from Aladdin with a purity greater than 98% and did not require further purification in the experiment. The chemical structure of DPD molecule is shown in Fig. 1. The iron content of the X60 steel was 99.9%. The steel area was 1 cm^2 when used as a working electrode and the electrode was mechanically polished to 2000 sandpaper and sonicated with deionized water to remove contaminants before performing electrochemical experiments. Concentrated hydrochloric acid was diluted to 1 M as the corrosion medium for X60 steel.

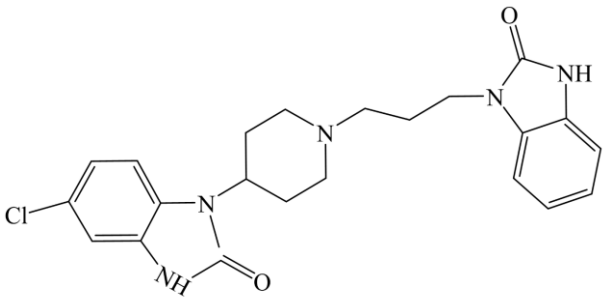

Figure 1. Chemical structure of Domperidone

2.2 Electrochemical experiment

The gamry600+ instrument was used for electrochemical experiments and a standard three-electrode cell assembly was used for this purpose. The electrochemical data obtained were analyzed using Zsimpwin software. In the electrochemical experiments, X60, saturated glycerol electrode (SCE)

and platinum sheet were used as working electrode, reference electrode and counter electrode, respectively. The electrochemical impedance spectrum (EIS) experiments were performed with an amplitude of 10 mV in the frequency range of 100 kHz ~ 10 mHz. Potentiodynamic polarization measurements were performed by scanning the potentials from 250 mV / E_{OCP} to +250 mV / E_{OCP} at a constant scan rate of 1 mV s^{-1}. All potentials reported below are related to SCE.

2.3 Surface Analysis

The surface morphology of X60 specimens immersed in hydrochloric solutions without and with DPD corrosion inhibitors for five hours was examined by field emission scanning electron microscopy (FE-SEM).

2.4 MD calculation

Molecular dynamics simulations were used to study the adsorption behavior of DPD on the Fe (110) surface. The Fe (110) surface was chosen to simulate the adsorption process because of its high density and stability. Simulations were carried out for (24.3,17.2,62.5) Å of the Fe (110) surface, each layer containing one DPD molecule and 200 water molecules at 298 K NVT. Molecular dynamics was used to calculate the low conformational adsorption energy for the interaction of the corrosion inhibitor molecules with the two surfaces of the aqueous phase.

3. RESULTS AND DISCUSSION

3.1 Electrochemical testing

Fig. 2 shows the OCP curves of X60 in 1 M HCl in the absence and presence of DPD at 298 K. From the OCP curves, it can be seen that the OCP values of X60 in hydrochloric acid solution stabilize after a period of time. After adding DPD corrosion inhibitor to the hydrochloric acid solution, the OCP value became larger, indicating a smaller tendency of self-corrosion, and the largest change in OCP value was observed after adding DPD of 400 mg/L, indicating that X60 suffered the least corrosion at this concentration. This change in behavior may be due to the adsorption of DPD molecules on the surface of X60 steel, forming a protective film.

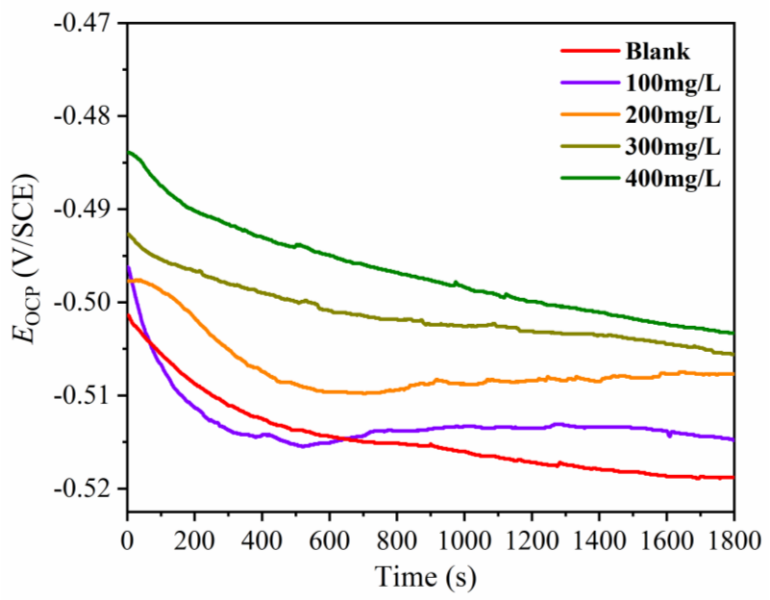

Figure 2. OCP curves for X60 in 1 M HCL without and with DPD at 298K

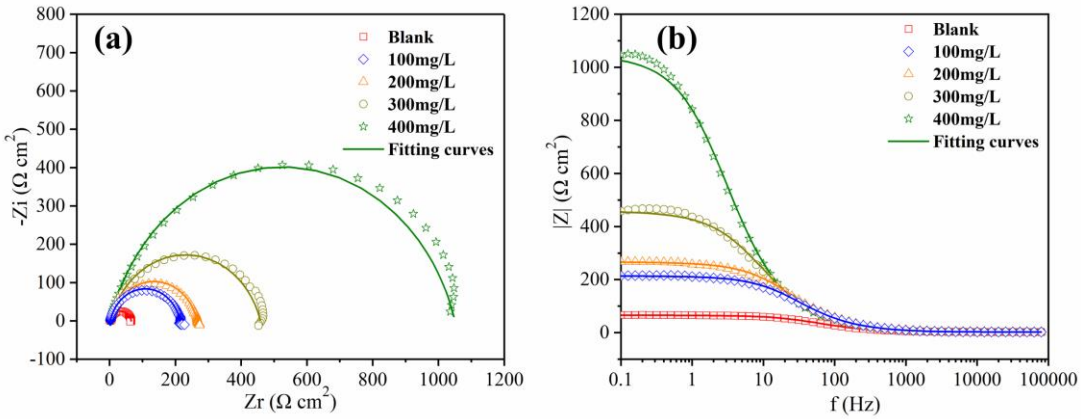

Figure 3. Nyquist plots (a) and bode plots (b) for X60 in 1 M HCL without and with DPD at 298K

The corrosion behavior of X60 steel at 298K was evaluated by adding different concentrations of DPD to the hydrochloric acid solution using EIS. The obtained Nyquist plots are presented in Fig. 3. The shape of the Nyquist diagram does not change with or without the addition of DPD corrosion inhibitor to the hydrochloric acid solution. In the tested frequency range, there is only one depressed capacitive imperfect semicircle, indicating that corrosion reactions are usually controlled by charge transfer processes on heterogeneous and irregular steel surface electrodes [24-26]. In addition, the semicircle diameter increased with increasing DPD addition concentration, indicating a more effective protection of the steel electrode [27, 28].

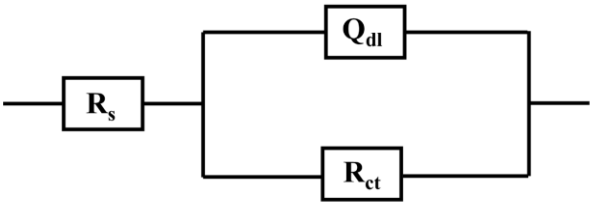

Figure 4. Equivalent circuit model of the X60 electrodes in 1 M HCL solution

The equivalent circuit model by fitting a Nyquist plot was obtained in Fig. 4. In the model, R_s denotes the solution resistance, R_{ct} represents the charge transfer resistance and constant phase element (CPE) is used instead of capacitive components. The impedance of CPE is described as follows [29-31] **:**

$$Z_{cpe}=1/(Y_0(j\omega)^n) \quad (1)$$

where j: the imaginary root, ω: the angular frequency, Y_0: proportional factor, and n: the CPE index associated with the inherent chemical and physical heterogeneous characters of the solid surfaces. The CPE can show a resistor (n = 0), a Warburg impedance (n = 0.5), or a capacitor (n = 1).

The relevant parameters for impedance are listed in Table 1. The inhibition efficiency can be calculated by the following equation:

$$\eta\ (\%) =(R_{ct}-R_{ct}^0)/R_{ct}\times 100\% \quad (2)$$

where R_{ct} and R_{ct}^0 are the transfer resistances in the presence and absence of DPD, respectively. As can be seen from Table 1, the R_{ct} values increased significantly with increasing DPD concentration, which was due to the formation of a protective film on the X60 surface. This behavior can be explained by the increase of corrosion inhibitor adsorbed on the X60 surface, reducing the charge transfer between the X60 steel surface and the corrosive medium [32, 33]. When 400 mg/L corrosion inhibitor was added into hydrochloric acid solution, the best protection performance of X60 steel was 93.96%.

Table 1. Electrochemical impedance parameters obtained for X60 in 1 M HCL without and with DPD at 298K

C (mg/L)	R_s (Ω cm^2)	R_{ct} (Ω cm^2)	CPE ($10^{-4}\Omega^{-1}s^n cm^{-2}$)	n	η (%)
0	2.5	63.3	1.38	0.85	
100	2.3	211.8	0.69	0.85	70.14
200	2.4	263.9	0.73	0.84	76.03
300	2.4	456.3	1.01	0.82	86.14
400	2.4	1047.0	1.10	0.83	93.96

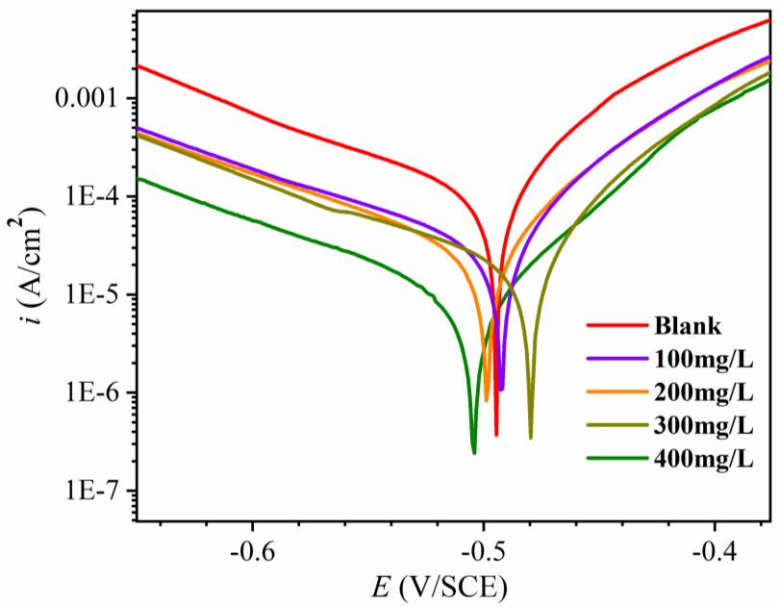

Figure 5. Potentiodynamic polarization curves for X60 in 1 M HCL solution without and with DPD at 298K

In order to further evaluate the protective effect of DPD inhibitors on X60 steel, the polarization technique was investigated. The potentiodynamic polarization curves of the steel at different concentrations of DPD in the presence of 1 M HCl solution at 298 K are shown in Fig. 5, and the relevant parameters (corrosion potential (E_{corr}), corrosion current density (i_{corr}), anodic (β_a), cathodic (β_c) Tafel slopes) of the polarization curves are given in Table 2. The percentage inhibition efficiency η % is given by the following equation (3):

$$\eta\ (\%) = (i_{corr,0} - i_{corr})/(i_{corr,0}) \times 100\% \quad (3)$$

It can be seen from the figure that the cathode curve is relatively parallel after the addition of DPD corrosion inhibitor, indicating that the effect of DPD corrosion inhibitor on the cathode is small and the effect of metal dissolution on the anode is more significant [34, 35]. With the increase of DPD concentration, the corrosion current density decreases. This is due to the adsorption of the corrosion inhibitor at the X60 steel/acid solution interface reducing the dissolution of the steel [36, 37]. At a concentration of 400 mg/L, the corrosion inhibitor efficiency reaches 93.34%, which achieves the best protection. The maximum shift of the E_{corr} value in the tested polarization curve was 9.5 mV, indicating a mixed action of the DPD corrosion inhibitor [38-41].

Table 2. The polarization parameters obtained for X60 in 1 M HCL without and with DPD at 298K

C (mg/L)	E_{corr} (mV/SCE)	i_{corr} (μA cm^{-2})	β_a (mV dec^{-1})	β_c (mV dec^{-1})	η (%)
0	−495	98.41	49	−113	
100	−493	31.48	49	−127	68.01
200	−499	24.22	54	−114	75.39
300	−480	17.67	45	−153	82.04
400	−504	6.55	49	−89	93.34

3.2 SEM analysis

The morphology of X60 steel surface immersed in hydrochloric acid solution with and without DPD corrosion inhibitor was observed using FE-SEM and the results are shown in Fig. 6. In the absence of the DPD inhibitor, Fig. 6a shows that the surface of the X60 in the hydrochloric acid solution is quite rough and exhibits a fish scale morphology accompanied by the formation of corrosion products due to the corrosion of the hydrochloric acid solution. On the other hand, with the addition of DPD molecules to the hydrochloric acid solution, the surface of the exposed steel specimens is smooth and scratches from mechanical polishing can also be seen, indicating the formation of a protective film on the X60 surface from the adsorption of inhibitor molecules.

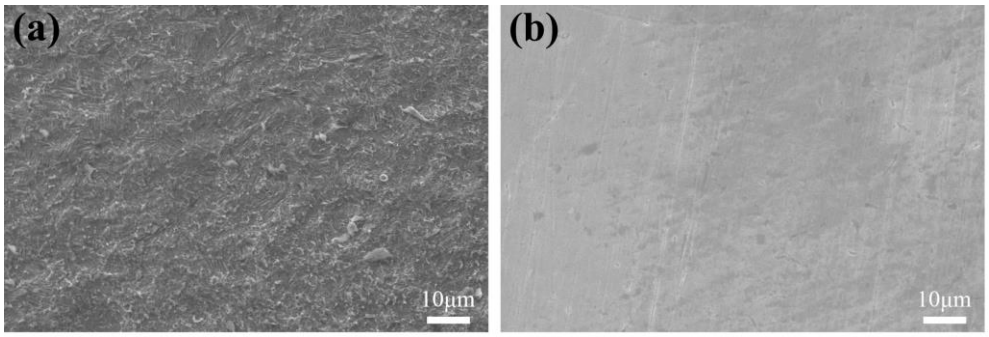

Figure 6. SEM images of bare X60 (a) and with 400 mg/L DPD (b) after being immersed in 1 M HCL solution for 5h

3.3 Adsorption isotherm

In order to understand the mode of interaction of corrosion inhibitors with metal surfaces, it is necessary to utilize adsorption isotherms. In this study, the Langmuir adsorption isotherm was fitted to investigate the adsorption behavior of DPD corrosion inhibitors on the surface of X60 steel. The Langmuir isotherm can be expressed by the following equation [42]:

$$C/\theta = 1/K_{ads} + C \quad (4)$$

where C denotes the concentration of the inhibitor, K_{ads} represents the adsorption equilibrium constant, and θ (surface coverage) is defined as the corrosion inhibition efficiency obtained from the polarization curve measurements. Fig. 7 shows C vs C/θ as a straight line with a correlation coefficient (R^2) of 0.98866 and a slope of 0.94. The larger the value of K_{ads} calculated from the isotherm intercept, the stronger the interaction of the corrosion inhibitor molecules with the metal surface. The K_{ads} correlates with the standard free energy of adsorption (ΔG^0_{ads}) as follows:

$$K_{ads} = 1/C_s \, exp\left(\frac{-\Delta G^0_{ads}}{RT}\right) \quad (5)$$

where, R is the molar gas constant (8.314 J mol $^{-1}$ K $^{-1}$) and T is the absolute temperature (K), C_s corresponds to the concentration of water in solution (1×10^3 g/L). The calculated Gibbs free energy is about −24.03 kJ mol^{-1}. Negative ΔG^0_{ads} value indicate that the adsorption process of DPD molecules on the steel surface is spontaneous [43]. Generally speaking, ΔG^0_{ads} value less than −20 kJ mol^{-1} is physical

adsorption and higher than −40 kJ mol^{-1} is chemisorption [44]. In the present case, the ΔG^{0}_{ads} value is in the middle range, indicating a combination of physical and chemical adsorption.

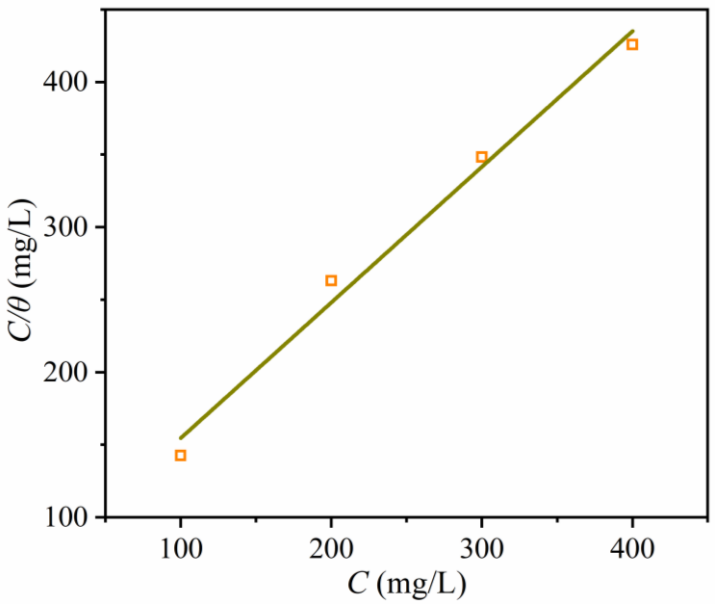

Figure 7. Langmuir adsorption plots of DPD on the X60 electrodes in 1 M HCl solution

3.4 Molecular dynamics calculation

The molecular dynamics calculations of DPD on Fe (110) was used to determine theoretically the adsorption configuration and adsorption energy of DPD molecules on the surface of X60 steel. The most stable low-energy configuration of DPD adsorption on the Fe (110) surface in the aqueous phase is shown in Fig. 8. As can be seen from the figure, the adsorption conformation of DPD molecules is parallel to the steel surface, which promotes effective surface residence and greater coverage, thus hindering the attack of aggressive ions during the immersion process[45-47]. The calculated DPD adsorption energy of −289.2 kJ mol^{-1} is much larger than the adsorption energy of water molecules on the steel surface of −74.08 kJ mol^{-1}, which indicates that DPD molecules can displace water molecules and form a protective film on the steel surface [15, 48, 49].

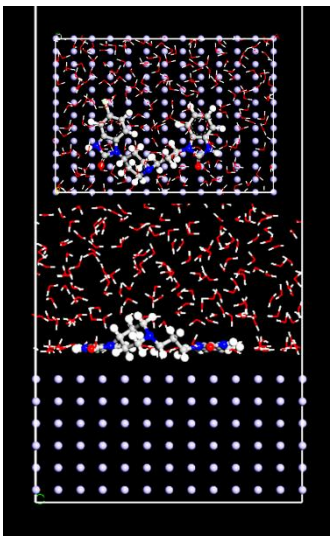

Figure 8. Equilibrium adsorption configuration of DPD molecule on Fe (110) substrate (inset: on-top view)

4. CONCLUSION

The inhibition effect of a drug molecule DPD on X60 carbon steel in a 1 M hydrochloric acid environment was investigated. The evaluation was achieved by electrochemical measurement techniques at 298 K. The inhibition efficiency of the DPD corrosion inhibitor on the steel was positively correlated with the amount added in the hydrochloric acid and the highest inhibition efficiency of 93.96% was achieved at a content of 400 mg/L. The surface morphology of the immersed specimens in the hydrochloric acid solution confirmed the electrochemical results. DPD molecule adsorption on the steel surface followed the Langmuir adsorption theory and is a joint result of physical and chemical adsorption. Moreover, the optimal adsorption configuration of DPD molecules on the steel surface was calculated by molecular dynamics.

ACKNOWLEDGMENTS
This work was partly sponsored by the Foundation of the Department of Science and Technology of Guizhou province (QKHPTRC[2021]5643).

References

1. I.B. Obot, A. Madhankumar, *J. Ind. Eng. Chem.*, 25 (2015) 105-111.
2. L.O. Olasunkanmi, I.B. Obot, M.M. Kabanda, E.E. Ebenso, *J. Phys. Chem. C.*, 119 (2015) 16004-16019.
3. B. Hou, X. Li, X. Ma, C. Du, D. Zhang, M. Zheng, W. Xu, D. Lu, F. Ma, *NPJ. Mater. Degrad.*, 1 (2017).
4. H. Li, Y. Qiang, W. Zhao, S. Zhang, *Corros. Sci.*, 191 (2021) 109715.
5. Y. Qiang, H. Zhi, L. Guo, A. Fu, T. Xiang, Y. Jin, *J. Mol. Liq.*, 352 (2022) 118638.

6. Y. Qiang, S. Zhang, S. Xu, W. Li, *J. Colloid. Interf. Sci.*, 472 (2016) 52-59.
7. Q. Deng, N.-N. Ding, X.-L. Wei, L. Cai, X.-P. He, Y.-T. Long, G.-R. Chen, K. Chen, *Corros. Sci.*, 64 (2012) 64-73.
8. Y. Qiang, S. Xu, L. Guo, N. Chen, Ime B. Obot, *Int. J. Electrochem. Sci.*, 11 (2016) 3147-3163.
9. Marija B. Petrović Mihajlović, Milan M. Antonijević, *Int. J. Electrochem. Sci.*, 10 (2015) 1027-1053.
10. Z. Chen, Z. Liu, K. He, G. Han, Y. Lv, J. Han, X. Wei, *Int. J. Electrochem. Sci.*, 16 (2021) 210559.
11. C. Li, Z. Sun, M. Kang, Z. Yan, Z. Tan, Q. Li, W. Wang, *Int. J. Electrochem. Sci.*, 16 (2021) 211034.
12. X. He, J. Mao, Q. Ma, Y. Tang, *J. Mol. Liq.*, 269 (2018) 260-268.
13. P. Kannan, T.S. Rao, N. Rajendran, *J. Colloid. Interf. Sci.*, 512 (2018) 618-628.
14. E. Naseri, M. Hajisafari, A. Kosari, M. Talari, S. Hosseinpour, A. Davoodi, *J. Mol. Liq.*, 269 (2018) 193-202.
15. M. Abdallah, *Corros. Sci.*, 46 (2004) 1981-1996.
16. M.M. El-Naggar, *Corros. Sci.*, 49 (2007) 2226-2236.
17. I.B. Obot, N.O. Obi-Egbedi, S.A. Umoren, *Corros. Sci.*, 51 (2009) 1868-1875.
18. S.K. Shukla, M.A. Quraishi, *Corros. Sci.*, 51 (2009) 1007-1011.
19. A.K. Singh, M.A. Quraishi, *Corros. Sci.*, 52 (2010) 152-160.
20. S. Bashir, V. Sharma, H. Lgaz, I.-M. Chung, A. Singh, A. Kumar, *J. Mol. Liq.*, 263 (2018) 454-462.
21. R.A. Anaee, I.H.R. Tomi, M.H. Abdulmajeed, S.A. Naser, M.M. Kathem, *J. Mol. Liq.*, 279 (2019) 594-602.
22. Y. Qiang, L. Guo, H. Li, X. Lan, *Chem. Eng. J.*, 406 (2021) 126863.
23. Y. Qiang, S. Zhang, L. Guo, S. Xu, L. Feng, I.B. Obot, S. Chen, *J. Clean. Prod.*, 152 (2017) 17-25.
24. Y. Qiang, S. Zhang, L. Guo, X. Zheng, B. Xiang, S. Chen, *Corros. Sci.*, 119 (2017) 68-78.
25. H. Li, S. Zhang, Y. Qiang, *J. Mol. Liq.*, 321 (2021) 114450.
26. N. Yilmaz, A. Fitoz, ÿ. Ergun, K.C. Emregül, *Corros. Sci.*, 111 (2016) 110-120.
27. P. Dohare, K.R. Ansari, M.A. Quraishi, I.B. Obot, *J. Ind. Eng. Chem.*, 52 (2017) 197-210.
28. A. Dutta, S.K. Saha, U. Adhikari, P. Banerjee, D. Sukul, *Corros. Sci.*, 123 (2017) 256-266.
29. A. Espinoza-Vázquez, F.J. Rodríguez-Gómez, B.I. Vergara-Arenas, L. Lomas-Romero, D. Angeles-Beltrán, G.E. Negrón-Silva, J.A. Morales-Serna, *RSC Adv.*, 7 (2017) 24736-24746.
30. H. Li, S. Zhang, B. Tan, Y. Qiang, W. Li, S. Chen, L. Guo, *J. Mol. Liq.*, 305 (2020) 112789.
31. A. Zarrouk, B. Hammouti, A. Dafali, F. Bentiss, *Ind. Eng. Chem. Res.*, 52 (2013) 2560-2568.
32. M. Bozorg, T. Shahrabi Farahani, J. Neshati, Z. Chaghazardi, G. Mohammadi Ziarani, *Ind. Eng. Chem. Res.*, 53 (2014) 4295-4303.
33. Y. Qiang, S. Fu, S. Zhang, S. Chen, X. Zou, *Corros. Sci.*, 140 (2018) 111-121.
34. Y. Qiang, S. Zhang, B. Tan, S. Chen, *Corros. Sci.*, 133 (2018) 6-16.
35. C. Verma, L.O. Olasunkanmi, T.W. Quadri, E.-S.M. Sherif, E.E. Ebenso, *J. Phys. Chem. C.*, 122 (2018) 11870-11882.
36. Y. Qiang, S. Zhang, H. Zhao, B. Tan, L. Wang, *Corros. Sci.*, 161 (2019) 108193.
37. I. Rotaru, S. Varvara, L. Gaina, L.M. Muresan, *Appl. Surf. Sci.*, 321 (2014) 188-196.
38. J.H. Al-Fahemi, M. Abdallah, E.A.M. Gad, B.A.A.L. Jahdaly, *J. Mol. Liq.*, 222 (2016) 1157-1163.
39. S.M. Azab, A.M. Fekry, *J. Alloy. Compd.*, 717 (2017) 25-30.
40. H. Lgaz, R. Salghi, S. Jodeh, B. Hammouti, *J. Mol. Liq.*, 225 (2017) 271-280.
41. M. Ramezanzadeh, G. Bahlakeh, B. Ramezanzadeh, Z. Sanaei, *J. Ind. Eng. Chem.*, 77 (2019) 323-343.
42. S. Ralkhal, T. Shahrabi, B. Ramezanzadeh, G. Bahlakeh, *Appl. Surf. Sci.*, 464 (2019) 178-194.
43. Y. Qiang, S. Zhang, S. Yan, X. Zou, S. Chen, *Corros. Sci.*, 126 (2017) 295-304.
44. L. Guo, I.B. Obot, X. Zheng, X. Shen, Y. Qiang, S. Kaya, C. Kaya, *Appl. Surf. Sci.*, 406 (2017) 301-306.

45. Y. Qiang, S. Zhang, L. Wang, *Appl. Surf. Sci.*, 492 (2019) 228-238.
46. Y. Qiang, H. Li, X. Lan, *J. Mater. Sci. Technol.*, 52 (2020) 63-71.
47. J. Haque, K.R. Ansari, V. Srivastava, M.A. Quraishi, I.B. Obot, *J. Ind. Eng. Chem.*, 49 (2017) 176-188.